Simulations of Diagnostic Emission due to Fuel-Pusher Mixing in Laser-Driven Implosions

It is important to develop diagnostics of the Rayleigh-Taylor instability that occurs during the deceleration phase of inertial-confinement-fusion capsule implosions because this instability is a crucial factor limiting the capsule performance.[1] To simulate the effects of this instability and to assess possible diagnostic techniques, a mix model has been added to the one-dimensional (1-D) hydrocode *LILAC*.[2] This model includes the effects of turbulent mixing on the hydrodynamic motion as well as on the temperature and material-concentration profiles within the plasma. In the work described here, this model is used to simulate time-resolved images of implosions of a gas-filled capsule that is representative of the kind proposed for near-term experiments on the 30-kJ, 60-beam OMEGA laser. In particular, the use of emission from thin chlorine-doped layers in the pusher is considered as a means to track the growth of the mixed region near the fuel-pusher interface. It is shown how the onset of mix-induced emission varies over a series of polymer-shell targets that are identical, except that the additive layer is displaced by different amounts from the fuel-pusher interface in each target. It is also shown that the introduction of an additive layer sufficiently thick to produce adequate diagnostic emission has a minor effect on the implosion performance, compared with the effects of mix itself.
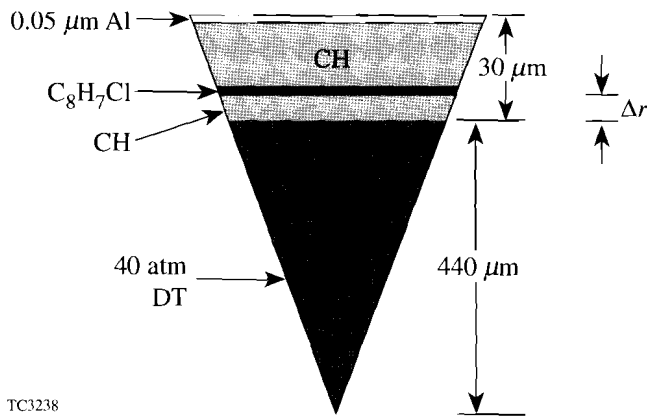
The Rayleigh-Taylor instability is the tendency of adjacent fluid layers to interpenetrate one another when the less dense of the two layers supports the denser layer under a gravitational or inertial force.[3] Under these circumstances, perturbations in their interface grow into buoyant bubbles of the lighter fluid that rise past sinking spikes of the heavier fluid.[4] As the depth of penetration becomes comparable to the lateral scale length of the bubble-spike structure, the interpenetration becomes more turbulent[4] and the state of the two fluids approaches that of a mixture.

This instability appears twice during a capsule implosion. The first occurrence, the acceleration-phase instability, starts at the very beginning of the implosion at the ablation front where the shell is being accelerated inward by the hot and relatively light plasma ablating from the capsule surface. This instability can be seeded by both initial surface imperfections in the shell and nonuniform laser irradiation. The second occurrence, the deceleration-phase instability, begins as the rising pressure in the fuel core decelerates the imploding shell. At this time, the inward radial acceleration reverses, and the instability moves to the inner side of the density peak in the pusher to the fuel-pusher interface, where the hot central fuel mass supports the cooler and denser pusher. Here, the unstable growth of the fuel-pusher interface is seeded by the accumulated distortion that feeds through from the ablation region. As pusher material mixes with the fuel, cooling by dilution causes the nuclear reaction rates to drop. In addition, the dispersal of the fuel into the pusher reduces the areal density of the fuel mass (the fuel-averaged density-radius product, ρR), which is a key measure of how close to ignition the fuel has come. If the pusher contains a substance other than hydrogen, radiative losses will cool the fuel further. If this enhanced radiation loss can be observed either spectroscopically or with imaging, then it can be interpreted as evidence that mix has occurred.

Such a diagnostic represents a logical extension of the technique of using plastic-coated glass targets[5] and multilayer targets[6] in thermal transport experiments to measure the advance of the thermal front in the ablation region. Calculations of the growth of the mix region near the ablation front showed that mixing due to the acceleration-phase instability significantly augments thermal conduction in transporting the laser-driven heat front to the glass substrate layer, which accounted for emission from the glass appearing sooner than expected from simulations based on thermal transport alone.[6]

In adapting this technique to the deceleration-phase instability of the fuel-pusher interface, we consider a series of targets where a thin additive layer is placed at various distances Δr from the inner surface of the pusher (see Fig. 64.18). The characteristic emission from the additive is delayed until the mixed region has grown through the underlying pure-CH polymer to include the additive layer. By measuring the delay

Figure 64.18
Section of the representative spherical capsule that will serve as the example in the calculations to follow. The C_8H_7Cl additive layer is 2-μm thick. It is to be imploded with a square 13.5-TW pulse of 2.3-ns duration.

of the additive emission as a function of the initial position of the additive layer, the trajectory of the bubble surface, the outer boundary of the mixed region, can be inferred.

This technique is also a refinement of a method used in experiments on the Nova laser at the Lawrence Livermore National Laboratory where iodine was added to polymer shells to increase the emissivity of the pusher.[7] In other experiments,[8] chlorine was used as a pusher additive and argon as a fuel additive. The overall degree of mixing was inferred from the intensity of chlorine emission, relative to the intensity of the argon emission, and an average temperature of the mixed additive was obtained from the line ratios of the spectra of the additives. The use of thin additive layers and time-resolved measurements allows the growth of the mix region to be followed in time by associating the arrival of the outer mix-region boundary at the additive-layer radius with the onset of the characteristic additive emission. The idealizations of a distinct mix-region boundary at the bubble front and an abrupt onset of the diagnostic emission are only approximations, but they are useful for understanding the results of the simulations and for anticipating the results of actual experiments.

Mix Modeling in One Dimension

In our spherically symmetric, purely 1-D simulation, the multidimensional bubble-spike structure and the subsequent turbulent structure are not described explicitly, leaving instead a fluid that is completely mixed at the atomic level. The mix model used within the 1-D hydrocode *LILAC* is formulated as

a diffusive process that transports constituent concentrations and thermal energy within the boundaries of the mix region. These boundaries are the bubble and spike fronts obtained from perturbation mode amplitudes calculated from the 1-D hydrodynamics using a multimode Rayleigh-Taylor model similar to that of Haan.[9] The diffusion coefficient is the product of a velocity derived from the expansion of the mix region and a scale length λ_{mix} characteristic of the mixing motion. At this point in the development of the 1-D mix model, this scale length is a free parameter, but work is now in progress to allow its value to be derived at each time from other physical parameters of the system being simulated. The inclusion of this 1-D mix model within *LILAC* allows for simulations that take into account the cooling effects of radiation and dilution and the associated reduction in the diagnostic emission and the neutron yield. These simulations also allow the hydrodynamics to respond to the moderated density and pressure profiles, as well as to the effects of the modified radiative properties of the mixed fluid.

An important consequence of this 1-D approximation is that the interpenetrating fluid elements share the same spherically averaged temperature profile. It is reasonable to expect that thermal conduction equilibrates temperatures rapidly over the short scale lengths of the interpenetrating fluid bubbles, spikes, fingers, and eddies, which will tend to evolve the temperature of the mixing region toward a spherically symmetric temperature profile common to all the constituents. To the extent that this is true, the temperature in the neighborhood of a particular ion of additive material will depend more on its radial coordinate than on information lost by disregarding the nonspherical fluid structure.

A difficulty with the 1-D mix model can occur when the mixed region is optically thick. In reality, or in a multidimensional description, this region could have optically thin spots that would allow radiation to escape that otherwise would not escape. Even a relatively subtle effect of this kind would limit the usefulness of a 1-D model for simulating quantitative line intensities, except when line-absorption effects are negligible or otherwise well understood. Also, emission that is particularly temperature sensitive could be misrepresented if spherical averaging were to smooth out some hot spots. However, the use of a local transport model in 1-D does preserve important elements of realism by evolving and distributing the constituent concentrations in a physically plausible way. This is an improvement over global approximations such as forcing flat concentration profiles throughout the mix region[8] or postulat-

ing analytical forms to interpolate the temperature, density, and concentration profiles between the boundaries of the mixed region. Modeling the mix of thermal energy along with the plasma constituents gives an effective enhancement of thermal transport consistent with the mix model. Also, by incorporating the mix model into the hydrodynamics, the mix-affected plasma profiles and pressure gradient remain consistent with the main hydrodynamic process that is the formation of the compressed core.

Time-Dependent Pusher Emission

The capsule chosen to illustrate the model is shown schematically in Fig. 64.18. It is a 30-μm-thick CH polymer shell (the pusher), 940 μm in diameter, filled with 40 atm of DT. It is driven by a simple, flat-top, 13.5-TW pulse, 2.3 ns in duration. A 2-μm-thick layer of C_8H_7Cl is added to this basic design at a distance Δr from the initial pusher/fuel interface.

For illustrative purposes it is useful to talk of the onset of chlorine emission from this additive layer as a signal of the arrival of the bubble surface at the additive layer. This simplified interpretation is based on the assumption that the additive is heated to an emitting temperature immediately upon contact with the bubble front. However, the mix model used in the simulations makes no such assumption. It takes into account the delay required for the additive and the hot fuel to be transported into a common volume where a sufficient amount of additive can be brought to an emitting temperature so as to produce diagnosable radiation. Another simplification is to describe the mix region as having distinct boundaries. The mix model does employ such boundaries to delineate the mix region, but the actual modifications of the material content, temperature, and density profiles due to mix are obtained from a transport model.

Accepting for now this view that additive emission signals the arrival of the bubble front at the additive layer, Fig. 64.19 illustrates how the onset times of the additive emission can be used to track the trajectory of the bubble surface in a series of shots using capsules that are identical, except that the initial position Δr of the additive layer is varied. This figure shows the trajectories of the DT/CH interface and Lagrangian markers at various Δr's, together with the bounds of the predicted mixing region for two different surface finishes, for the illustrative capsule. The bounds of the mixing region correspond to the bubble and spike trajectories and are obtained as described above from the multimode Rayleigh-Taylor perturbation model adapted from the work of Haan.[9] Superimposed over the layer interface trajectories, they illustrate how the mixed region
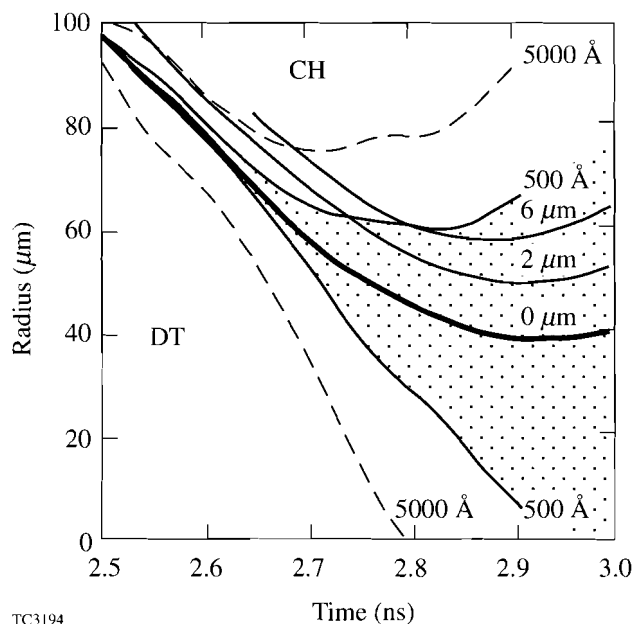

Figure 64.19
Calculated trajectories of the DT/CH interface (heavy line) and Lagrangian markers in the CH at initial distances Δr of 2 μm and 6 μm from this interface. The curves labeled 500 Å and 5000 Å indicate the bounds of the predicted regions of DT-CH mixing for these initial rms surface finishes. The mix region includes both hot core material and relatively cool pusher material. Diagnostic emission from an additive layer in the pusher can occur when it is heated by contact with hot fuel in the mix region.

grows to include both hot core material and additive at times that depend on the initial perturbation and on the initial location of the additive layer. In the calculations for Fig. 64.19, the mix diffusion step has been omitted from the hydrodynamics. The feedback of mix on the hydrodynamics has potentially important effects on the amount of additive emission, but its effect on the trajectories shown here is small.

The heavy curve labeled 0 μm is the trajectory of the decelerating fuel-pusher interface. The zero of the time axis is the time of the start of the laser pulse. The curves labeled 2 μm and 6 μm are trajectories that would have been taken by additive layers if they had been displaced initially by these distances from the inner surface of the shell. The pair of curves labeled 500 Å are the mix-front trajectories calculated assuming an initial rms perturbation amplitude equal to this value whose modal decomposition is of the form $l^{-5/4}$, where l is the spherical mode index. The dashed curve shows the much larger mixed region resulting from a 5000-Å surface perturbation. This rms perturbation amplitude should be comparable to an equivalent surface roughness, but a quantitative relationship

between surface roughness and the perturbation amplitude is not established at this time. Consequently, these results should be regarded as purely illustrative and not indicative of the performance of a capsule made to any given specification. Also, the relationship of this surface perturbation to an equivalent irradiation nonuniformity has not been determined.

The amplitudes of the fuel-pusher perturbation modes are set at the beginning of the shell deceleration to values obtained from the corresponding ablation-region mode amplitudes by applying the attenuation factor $\exp\left(-l\,\Delta r_s/r_a\right)$, mode by mode, where r_a is the radius of the ablation surface and Δr_s is the separation between the ablation surface and the fuel-pusher interface. This is the prescription suggested by Haan[9] for initializing mode amplitudes at a surface whose unstable perturbations are seeded by the instability that has grown at another surface. The form of this coupling factor corresponds to the decaying exponential dependence of the amplitude of a surface-wave eigenfunction on the distance from the perturbed surface. This correspondence is well motivated, but approximate, and requires further study.

For the purposes of illustration, then, the crossing of the trajectory of the bubble front with the trajectory of the additive layer can be taken to give the time when the additive material enters the mixed region. Presumably, the amount of hot fuel in the mixed region at this time has raised the temperature to a level sufficient for the additive to emit. Figure 64.20, which gives the functional dependence of this estimated emission onset time on the additive layer displacement Δr for a series of capsules with identical initial perturbations, shows that this onset time is delayed with more deeply inset additive layers and with smaller initial perturbations, as might be expected. Each curve was obtained from the bubble-front trajectory resulting from the corresponding initial surface perturbation. The points are the times at which this trajectory contacts an additive layer at the indicated initial displacement. Emission-onset timing data from an actual series of shots can be plotted in the same way. This data might not be so complete, however, because the onset time can be expected to become less distinct for additive layers inset by more than a few microns.

While Fig. 64.20 gives useful qualitative information, a mix transport model, such as the one described here, is required to provide more quantitative information. In particular, it can address the important questions of whether one obtains a coincidence of elevated temperature and additive concentration over a large enough volume to produce a signal that is distinct against the background of the polymer emission. This
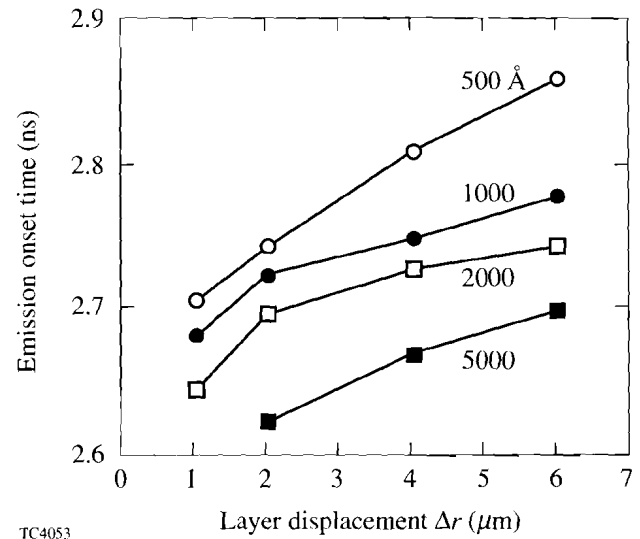

Figure 64.20
Time of onset of emission from the additive layer shown as a function of the initial additive layer displacement Δr from the inside surface of the polymer shell, for various initial surface perturbations.

article concentrates on the detection of additive emission by imaging. It is found that distinct time-dependent additive emission is obtained in the cases simulated here, although not for as full a range of additive layer displacements as is shown in Figs. 64.19 and 64.20.

Mix as a Diffusive Process

Once the growth and extent of the mix region have been obtained, a diffusive transport model is used to simulate the redistribution of the plasma constituents and thermal energy within this region. A natural way to regard mix in 1-D is that each zone in the numerical mesh exchanges a small amount of material with its closest neighbors at each time step. The finite-difference equation that describes this has the form of a diffusion equation. The diffusion coefficient is chosen to be the product of a mix velocity, taken from the velocities of the mix-region boundaries relative to the fluid velocities, and a mixing length. In all but one of the simulations described below, the mixing length is a free parameter. Results are obtained either for a fixed value chosen in advance or for a range of values to show how the outcome of the simulations can vary over the plausible limits of the model. "Flux limitation" is employed as well. The diffusive mass flux is forced to be less than a given multiple F of the free-streaming mass flux given by the product of the mass density and the mix velocity. This feature prevents unphysically large mass fluxes in the presence of large density gradients. The flux-limit parameter F is familiar from other

applications of diffusive transport[10] and is the second free parameter of this model. It is set equal to 2.0 in the calculations presented in this article. Once these two parameters are set, the concentration profiles of the mixed constituents and the mix-transported thermal energy density are then calculated in detail, according to local conditions, rather than from simpler unphysical and/or acausal assumptions such as instantaneous homogeneity within the mix region.

This model resembles the "k-ε" model in its use of diffusive transport to model turbulent transport,[11] but important differences exist. In the model used here, the momentum and kinetic energy of each fluid zone are conserved exactly, but there is no accounting for energy contained in the turbulent motion, in contrast to the k-ε model. Another difference is that this model contains a multimode instability calculation done in parallel with the mix transport, while the k-ε model includes no mode-spectral information. The mix-region model presented here offers the advantage of including the Haan multimode perturbation model with its phenomenology of the nonlinear growth of saturated modes. The spatial-spectral information kept by the multimode model is potentially important in the development of the mix-transport model beyond the version used to obtain the results shown below. For example, preliminary results have been obtained using a mixing scale length that is set equal to the rms perturbation wavelength averaged over the mode spectrum. This utilizes the spatial wavelength information in the perturbation mode spectrum, which is certainly a better strategy than using a fixed length chosen in advance. This derived scale length changes in time as the mode amplitudes themselves change and also as the transverse wavelengths of the individual modes decrease due to the mix region converging with the implosion.

An illustration of the direct effect of mix in 1-D simulations is provided by Fig. 64.21, which shows the spread of the concentration profile of the chlorine additive in the representative capsule shown in Fig. 64.18 for two values of Δr. In both cases the surface mass perturbation is set to 2000 Å with an $l^{-5/4}$ modal decomposition. Figure 64.21(a) shows the case where the initial additive layer is the innermost 2 μm of the pusher, and Fig. 64.21(b) shows the case where the additive layer is inset by 2 μm. The mixing length λ_{mix} is chosen to be 100 μm. In each case the sequence of concentration profiles includes the deceleration phase up to just beyond peak compression. In both cases the additive layers remain substantially undisturbed until after 2.4 ns. The additive layer at the fuel-pusher interface shows a slight preliminary dispersal. The main difference between the two cases occurs just after 2.5 ns, where the additive layer at the fuel-pusher interface begins to disperse about 100 ps before the inset additive layer. By 2.8 ns, the additive profiles have become nearly identical. The difference between the profiles between 2.5 and 2.7 ns suggests that the displacement of the additive layer by 2 μm can result in an effect that can be seen with a temporal resolution around the 100-ps level.

Effects of Mix on Capsule Performance

Simulating the emission from pusher additives requires mix modeling within hydrodynamic simulations to determine to what degree a given amount of additive perturbs the experiment, either by changing the hydrodynamic stability of the implosion or by quenching the diagnostic emission by dilution or by radiative cooling. The perturbative effect of a 2-μm additive layer at the inside surface of the shell can be evaluated from the results shown in Fig. 64.22 for implosions performed using a range of mixing scale lengths λ_{mix}. These simulations

TC3856
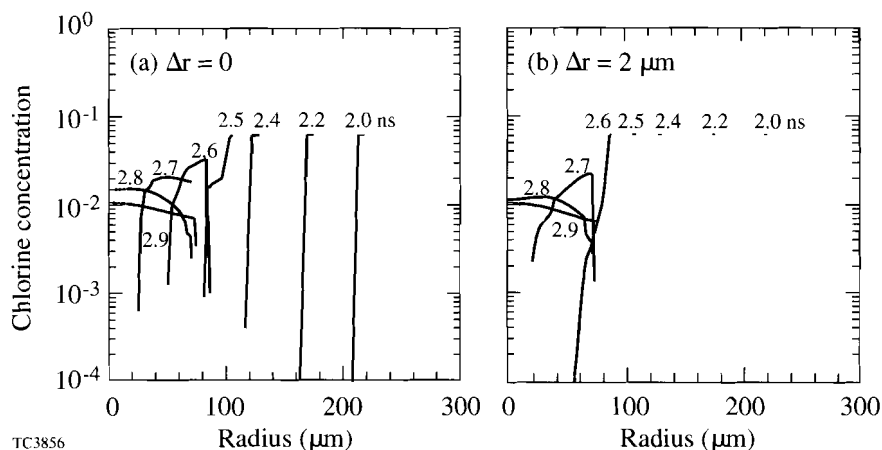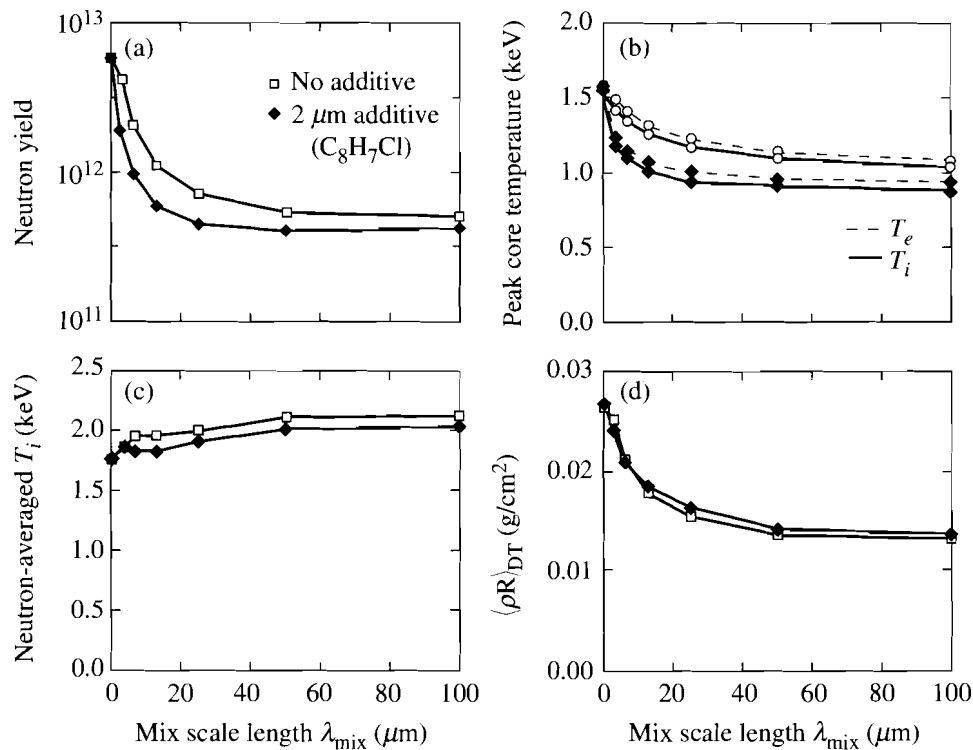
Figure 64.21
Sequences of chlorine concentration profiles for (a) $\Delta r = 0$ and (b) $\Delta r = 2$ μm. In each case the chlorine spreads as time increases, but the spreading is delayed, as expected, in the second case. These simulations were performed for an initial perturbation of 2000 Å and with $\lambda_{mix} = 100$ μm.

TC4054,4055,4056,4057

Figure 64.22

Effect of the diagnostic layer (2 μm of C_8H_7Cl) on (a) the neutron yield, (b) the peak electron and ion core temperatures, (c) the neutron-averaged ion temperature, and (d) the DT ρR. Results are plotted as a function of the mix scale-length parameter λ_{mix} for an initial surface perturbation of 2000 Å. The presence of the diagnostic layer is seen to have only a minor effect on the capsule behavior in comparison with the mix.

assume the same initial 2000-Å mass perturbation and $l^{-5/4}$ modal decomposition, which is severe enough to give a good indication of the worst-case effect of mix. The additive layer is placed at the fuel-pusher interface because this produces the maximum effect on the hydrodynamics. The mixing scale length is varied over the range from zero, which gives no mix at all, to 100 μm, where the net mixing rate is determined primarily by the flux limitation. In this case flux limitation restricts the speed of the mixing motion to no greater than 2.0 times the divergence speed of the bubble and spike surfaces, over and above the divergence of the 1-D fluid motion. Figure 64.22 shows that mix has a far greater impact on capsule performance than does the additive layer. Figure 64.22(a) shows that mix reduces the neutron yield substantially, corresponding to a small reduction in the ion temperature [which is shown in Fig. 64.22(b)]. The additional radiative cooling due to the additive is seen in Fig. 64.22(b) as a very slight additional reduction in temperature. Due to the strong dependence of the neutron-production rate on temperature, the effect of the addi-

tive on the total neutron yield is quantitatively significant, but it is clearly of secondary importance in comparison with the much greater effect of the much larger amount of pusher polymer that has been mixed in.

Figures 64.22(c) and 64.22(d) show the ion temperature and the peak value of $\langle \rho R \rangle_{DT}$, the radial integral of the DT mass density, both neutron averaged and thus relevant to nuclear diagnostics. The neutron-averaged ion temperature rises with mix due to the fact that quenching of neutron production within the mix region tends to shut off the yield from the cooler part of the core; this skews the neutron weighting of the temperature average toward the center of the capsule, which is hotter. The neutron-averaged ion temperature is not as sensitive to the presence of the additive as the neutron yield in Fig. 64.22(a). Note that $\langle \rho R \rangle_{DT}$ includes the DT mass only, wherever the mix might have taken it, and does not include the contribution of the pusher material. It is not the areal density of a distinct core. The neutron-averaged fuel areal density $\langle \rho R \rangle_{DT}$ de-

creases with increasing mix, but the additive has an almost negligible effect.

Figure 64.23 shows the neutron-production rates plotted as functions of time for a sequence of simulations with mixing lengths ranging from 0 to 100 μm. As above, this covers the range of mixing lengths from one that would give no mix at all to one that is large enough for the homogenizing effect of mix to be limited primarily by the flux limitation of the diffusion. A 2000-Å mass perturbation and $\Delta r = 0$ have been assumed in all cases. One striking aspect of the results shown in Fig. 64.23 is that the curves remain close to each other up to 2.6 ns where they abruptly diverge. Figure 64.21(a) shows that this is near the time when the entire inner 2 μm of pusher with the chlorine additive has just been drawn into the mix region, which is indicated by the tails on both ends of the concentration profile. By this time the mix region has expanded to include most of the fuel. This abrupt divergence of the neutron-production rates supports the interpretation that yield is effectively quenched by the arrival of pusher material, as was suggested above in explaining the results of Fig. 64.22.
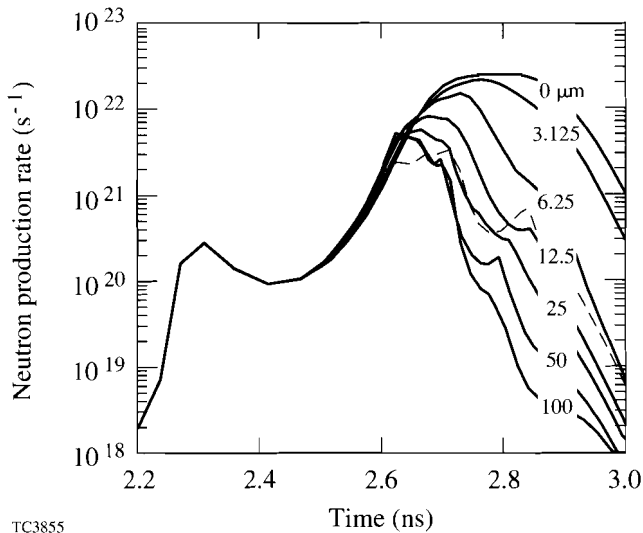

Figure 64.23
Neutron-production rate as a function of time for several values of the mix scale-length parameter λ_{mix}. The initial surface perturbation is 2000 Å. The dashed curve is obtained using a model where λ_{mix} is chosen to be equal to the time-dependent rms spherical wavelength of the perturbation mode spectrum.

The dashed curve in Fig. 64.23 is obtained using a time-dependent mixing length chosen to be equal to the rms spherical wavelength of the perturbation mode spectrum. This represents an attempt to reduce the number of *ad hoc* parameters in

the model. This choice of mixing length also results in an abrupt onset of quenching. The total yield obtained is very close to that obtained from the larger mixing lengths that give very rapid mixing, but later in the deceleration phase the neutron-production rate drops more slowly to values obtained at these later times with much shorter mixing lengths. This reflects the shortening of the average perturbation wavelength due to the spherical convergence of the mixing region, which in this case is a stronger effect than the tendency of the perturbation spectrum to evolve toward longer wavelengths as the shorter-wavelength perturbation modes saturate and fall behind the longer-wavelength modes.
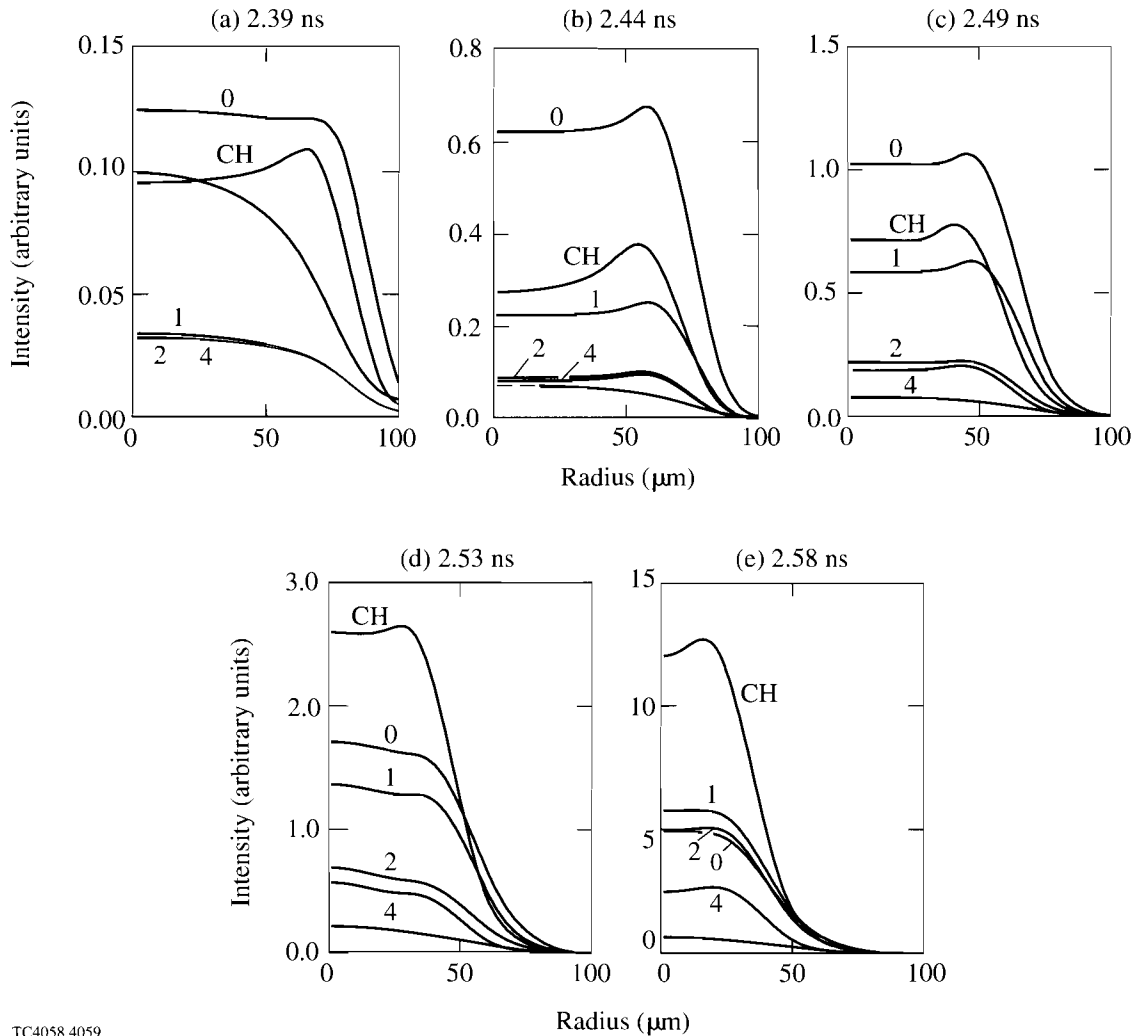
Effects of Mix on Images

Under conditions expected in the fuel-pusher mix, chlorine emission consists mostly of K-shell lines and bound-free continuum. Chlorine is distinctly more emissive than carbon under these conditions since carbon is then almost completely stripped and is seen mostly by its bound-free emission. Imaging implosions with emission in the 3- to 5-keV range isolates the chlorine continuum spectrally and enhances the contrast of emission from the hottest parts of the mixed region against the rest of the image. Chlorine is well suited as a pusher additive for the example described above because its K-shell lines occur just above the energies where the relatively cold pusher would attenuate emission from the center at times near peak compression. Avoidance of this attenuation is obviously important for observing mix with time-resolved spectroscopy.[12] The relative emission strength of chlorine over carbon allows small amounts of additive to be used. The detectability of the chlorine emission is limited by how well it competes with the continuum emission from the carbon, which is the main ingredient of the pusher and thus much more abundant. This is of particular concern when observing line emission from embedded additive layers since the additive lines must be observed against the background of continuum from all the carbon in the overlying layer of pure polymer.

Simulations of framing-camera images are obtained from integrating the equation of radiative transfer along straight-line photon paths through time-dependent emissivity and opacity profiles, taken from the 1-D hydrodynamic simulation, and into a model of a framing camera. The camera forms pinhole images on a photocathode. The images are transferred to a phosphor screen through a multichannel plate, which is triggered by a short electrical pulse propagating along a stripline over the plate. The model includes the camera geometry, the optics of finite pinholes, and a temporal response based on the calculated response of the multichannel plate to the electrical

pulse provided. The gating time is 45 ps, which represents a near-term development goal for this instrument. The intensity units in the plotted images are arbitrary since the camera model does not include information from an absolute calibration, but the relative intensities from frame to frame are consistent in these units. The spectral response of the camera includes that of the camera itself and foil filters of 25 μm of beryllium and 20 μm of titanium to center the net response within a window from about 3 to 5 keV.

Figure 64.24 shows a sequence of five framing-camera images, taken 50 ps apart, of the previously chosen polymer capsule with mix seeded by a 2000-Å exterior mass perturbation. The results from six simulations are superposed. Each curve represents the azimuthally averaged image intensity plotted as a function of radius. A mixing length of 100 μm is assumed. The value of the numeral labeling curves 0, 1, 2, and 4 is the initial displacement, in microns, of the additive layer outward from the inner surface of the pusher. The curve labeled

Figure 64.24
Simulated framing-camera images in the 3- to 5-keV range at times 45 ps apart ranging from (a) 2.39 ns to (e) 2.58 ns. The curves labeled 0 to 4 are for additive layer displacements of 0 to 4 μm, respectively; the curves labeled CH are for a pure CH pusher (no additive layer), and the dashed curves are for the case of no mix. Except for the dashed curves, the initial surface perturbation is 2000 Å and the mix scale-length parameter λ_{mix} is 100 μm. Note the different intensity scales.

"CH" corresponds to a calculation with no additive layer, and the dashed curve is obtained from a simulation of the case "0," where the additive layer is at the fuel-pusher interface and where no mix takes place.

At the time of the first frame [Fig. 64.24(a)], mixing has already begun. The effect of this is seen in the brightness of image 0 relative to the dashed line, its unmixed counterpart. A comparison of image 0 with image CH, obtained with no additive, shows that the additive results in a brighter image, as is expected, but without limb brightening, in contrast to the distinct limb brightening of the image CH. The intrinsic emissivities of both capsules are, in fact, peaked at their fuel-pusher interfaces, but at this early time there remains enough cool additive surrounding the fuel-pusher mix region of the additive-layer capsule to form an attenuating layer that rounds off the image by a limb-absorption effect. This limb darkening is particularly strong for images 1, 2, and 4, where the entire additive layer is cold and absorbing. The conditions at the fuel-pusher interfaces of these three cases are essentially identical to those of the CH case where there is no additive, and the differences between their images and that of the CH case are almost entirely due to this absorption. The nearly complete indistinguishability of the 1, 2, and 4 curves is evidence that the additive layer has no other effect on the implosion.

At later times curves 1, 2, and 4 brighten, in the expected order, as fuel-pusher mixing overtakes the additive layers successively further from the fuel-pusher interface. For example, from frame (d) to frame (e), curve 2 brightens to become comparable in intensity to curves 0 and 1. This systematic effect of the additive-layer displacement on the time dependence of the additive emission would be worth looking for in an actual experiment. These images tend to become more limb brightened as the additive becomes more emissive than absorbing, but there is a competing effect favoring central emission as well, as is seen in frame (d).

The five frames show that the fuel cores contract by a factor of about 2 for each calculation over the 200 ps shown. Nevertheless, there are subtle differences in their dynamics that are caused by mix. These effects, in combination with rapidly increasing intensities, add a potentially significant bias to the comparison of the overall intensities of any two images at any given instant. Comparing image intensities at points of equal core compression, for example, could give different results. Thus some caution is required in comparing relative intensities in Fig. 64.24. The CH images of the pure polymer capsule in particular appear surprisingly bright, relative to the images of

capsules with additive layers. The pure polymer capsule does, in fact, implode sooner than the additive-layer capsules and is found to reach peak compression about 30 ps earlier. Consequently, if the images were all compared at identical degrees of convergence, rather than at identical points in time, the intensity from the pure polymer capsule would be seen to be much more in line with those of the other images.

Relaxing the flux limitation by increasing the flux-limit parameter allows a greater concentration of chlorine to reach the spike front from the bubble front, and greater limb brightening is obtained. This is what would most likely result from a mix model that instantaneously homogenized all the material within the mix region, which is unphysical, at least from the point of view of the mix transport model used in this work.

Over the entire 200 ps spanned by these images, all the images brighten by nearly two orders of magnitude, except for the unmixed case, which lags far behind. This shows that mix can be expected to have a strong brightening effect on images of polymer-shell implosions, regardless of how they are modified by additive layers.

Conclusions

In conclusion, experiments are proposed to diagnose pusher/fuel mixing in imploding gas-filled capsules using additive layers of chlorinated plastic at various distances from the initial pusher/fuel interface. A mix model has been developed to simulate these experiments. The model includes the self-consistent modifications to the capsule hydrodynamics that result from a time-dependent diffusive treatment of the mix region. These experiments appear promising, based on the present analysis. The proposed diagnostic technique is, of course, compatible with other diagnostics suggested elsewhere, such as detailed line-shape and line-ratio analysis, with or without a fuel additive.

REFERENCES

1. J. Nuckolls, L. Wood, A. Thiessen, and G. Zimmerman, Nature 239, 139 (1972).

2. Laboratory for Laser Energetics Report No. 16, 1973 (unpublished); Laboratory for Laser Energetics Report No. 36, 1976 (unpublished).

3. Lord Rayleigh, *Scientific Papers* (Cambridge University Press, Cambridge, England, 1900), Vol. II, pp. 200–207; G. I. Taylor, Proc. R. Soc. Lond. A **201**, 192 (1950).

4. F. H. Harlow and J. E. Welch, Phys. Fluids **9**, 842 (1966).

5. J. Delettrez, Can. J. Phys. **64**, 932 (1986) and references cited therein.

6. J. Delettrez, D. K. Bradley, and C. P. Verdon, Phys. Plasmas **1**, 2342 (1994).

7. B. A. Hammel *et al.*, ICF, LLNL Quarterly Report **1**, (1991), pp. 151–156.

8. T. R. Dittrich *et al.*, Phys. Rev. Lett. **73**, 2324 (1994).

9. S. W. Haan, Phys. Rev. A **39**, 5812 (1989).

10. R. C. Malone, R. L. McCrory, and R. L. Morse, Phys. Rev. Lett. **34**, 721 (1975).

11. S. Gauthier and M. Bonnet, Phys. Fluids A **2**, 1685 (1990).

12. R. Epstein, J. A. Delettrez, C. P. Verdon, D. Shvarts, and B. Yaakobi, Bull. Am. Phys. Soc. **39**, 1695 (1994).